Marine DOC Modeling Suggests the Importance of Hydrothermal Vents and Initial DOC Production

A THESIS SUBMITTED TO THE FACULTY OF THE

UNIVERSITY OF MINNESOTA

BY

JACOB ZAHN

IN PARTIAL FULFILLMENT OF THE REQUIREMENTS

FOR THE DEGREE OF

MASTER OF SCIENCE

KATSUMI MATSUMOTO

JUNE 2021

Acknowledgements

This work was supported by the Department of Earth & Environmental Sciences and the US National Science Foundation (grant OCE-1827948 to K. Matsumoto). This work was carried out in part using computing resources at the University of Minnesota Supercomputing Institute. The temperature- and NPP-dependent export production scheme in MESMO 2 was coded by T. Tanioka.

Abstract

Marine DOC represents the largest ocean reservoir of reduced carbon, holding > 200 times the carbon inventory of marine biomass, or an amount of carbon roughly equal to that in the atmosphere. Therefore, the DOC reservoir is significant in terms of long-term climate change. The largest fraction of DOC is characterized as refractory (DOC_R) and radiocarbon ages indicate that this fraction survives multiple deep ocean mixing cycles. While DOC_R production is understood to be tied mainly to primary production in the surface ocean, the mechanisms for DOC_R removal are less well-understood, which has caused difficulty in quantifying the dynamics of this reservoir. However, photodegradation and hydrothermal vent degradation have been identified as likely mechanisms. In this study, DOC dynamics were incorporated into a well-calibrated dynamic ocean model, which explicitly represents important DOC processes: DOC production through primary production and degradation via photodegradation, hydrothermal vent degradation, and slow background degradation. A model simulation using literature values for key model parameters (Literature Value Run) resulted in large discrepancies from observation in both DOC concentration and the gradient in DOC concentration along the path of deep ocean circulation. These discrepancies suggest that the current state of knowledge of the underlying processes related to these observations is inadequate. After tuning model parameters, most notably DOC_R production and the flux of seawater through hydrothermal vents, a Tuned Run was achieved. From this run, sensitivity tests were performed to examine how dependent model results were to changes in key model parameters. Between the Literature Value Run, the Tuned Run, and the sensitivity tests, three conclusions were drawn: (1) it is likely that the current literature value for the fraction of NPP that becomes

DOC_R is too large, by approximately five times, (2) the literature value for hydrothermal vent flux is likely too small and may be five times the current value, and (3) hydrothermal vents are a likely source of radiocarbon-depleted DOC to the deep ocean.

Table of Contents

List of Tables

List of Figures

1. Introduction

At 662 Pg C, marine dissolved organic carbon (DOC) represents the largest ocean reservoir of reduced carbon, holding greater than 200 times the carbon inventory of living marine biomass (Hansell et al., 2009), or an amount roughly equivalent to that in the atmosphere (750 Pg C; Fasham et al., 2001). DOC refers to the carbon that is part of the more encompassing dissolved organic matter (DOM) pool, which also includes dissolved organic nitrogen (DON) and dissolved organic phosphorous (DOP). Operationally speaking, DOC is too small to sink through the water column and is therefore transported in the ocean passively by ocean circulation. Conversely, particulate organic carbon (POC) is large enough in size to sink through the water column. Marine DOC is believed to be produced autochthonously through photosynthesis in the surface ocean at a rate of ~27 Pg C yr^{-1} (Hansell, 2013), where it serves as a source of food for heterotrophic microbes. Chemosynthesis also contributes to DOC production, but the magnitude is thought to be small relative to photosynthesis. Most (25 Pg C yr^{-1}) of the freshly produced surface DOC is rapidly remineralized to carbon dioxide in the surface ocean as it supports heterotrophic respiration. The remainder of DOC escapes rapid remineralization and accumulates in the ocean over time scales of years to millennia.

DOC is eventually transported by ocean mixing below the biologically active surface (130 m) at a rate of approximately 1.9 Pg C yr^{-1}, ~20% of global export production (Laws et al., 2000; Dunne et al., 2007), and helps fuel heterotrophic metabolism in the upper mesopelagic (200-500 m). As a result, DOC exported below 500m is much smaller than at 130m (~0.2 Pg C yr^{-1}). Once DOC is exported to the deep ocean, it can be sequestered for centuries to millennia (Druffel et al, 1992). Due to the large size of the

DOC pool and its significant contributions to marine carbon sequestration, the controls on marine DOC production and degradation have important implications for regulating the global carbon cycle and thus climate (Walker et al., 2016a,b).

DOC exists as a complex mixture of hundreds of thousands of organic compounds with distinct chemistries and structures, and this complexity increases in the deep ocean (Dittmar & Stubbins, 2014). Hansell et al. (2009) approached this problem by modeling DOC as five fractions with lifetimes ranging from hours to millennia. The modeling work performed in the current study resembles the strategy of Hansell et al. (2009), but with two DOC fractions: semi-labile DOC (DOC_{SL}), which persists on the order of a few months to years; and refractory DOC (DOC_R), which persists on the order of thousands to tens of thousands of years. The sum of DOC_{SL} and DOC_R gives the total DOC (DOC_T). Labile DOC (DOC_L), which largely supports surface heterotrophic respiration, is not considered here because it is consumed as rapidly as it is produced and cannot be observed in nature as a result. In addition, its lifetime is too short to be captured in the model to be described below. The DOC_{SL} fraction supplements the DOC_L pool in supporting microbial production, and it is able to accumulate due to its longer lifetime relative to DOC_L, leading to a global DOC_{SL} inventory of ~6 Pg C (Hansell, 2013). Since DOC_{SL} accumulates, it is subjected to lateral transport via ocean circulation. DOC_{SL} can be vertically transported to some extent, but this export typically ends in the mesopelagic zone (<500 m) where DOC_{SL} is remineralized by subsurface microbial production (Abell et al., 2000). The DOC_R fraction has a significantly longer lifetime (centuries to millennia) relative to $DOC_{SL.}$ This causes DOC_R to exist ubiquitously in the global ocean, which results in a global inventory of ~630 Pg C (Hansell, 2013), roughly equal to the amount of carbon in the atmosphere.

Due to the absence of DOC_{SL} in the interior ocean, along with the persistent nature of DOC_R, DOC_T in the deep ocean (~40 μmol kg^{-1}) is considered to be composed entirely of DOC_R, while surface DOC_T is a combination of the background DOC_R signal (~40 μmol kg^{-1}) and DOC_{SL} (Hansell, 2013).

DOC_T exists in the ocean at concentrations ranging between ~34 and 80 μmol kg^{-1} (Fig. 2; Hansell, 2013). DOC_T concentrations are highest in the euphotic zone where DOC_T is produced and where DOC_{SL} accumulates. Within the euphotic zone, DOC_T concentrations are highest in the most productive waters, typically along the eastern upwelling margins of ocean basins (Dittmar & Stubbins, 2014). Elevated DOC_T concentrations are also found in subtropical gyres, where long residence times combined with low nutrient levels allow DOC_T to accumulate without being rapidly remineralized. In addition, surface waters with strong vertical stratification (and therefore a shallow mixed-layer depth), such as those at mid and low latitudes, allow for more DOC_T accumulation and typically exhibit concentrations between 65-80 μmol kg^{-1} while higher latitudes typically have lower DOC_T concentrations (~40-50 μmol kg^{-1}) due to dilution caused by deeper vertical mixing (Hansell, 2013). Globally, DOC_T concentration attenuates with depth until approximately 1,000 meters, below which concentrations remain stable at ~35-40 μmol kg^{-1} (Fig. 2; Hansell, 2013). However, a distinct gradient in DOC_T concentration (29% reduction in concentration) exists along the deep ocean pathway from the North Atlantic to the North Pacific (Druffel et al., 2016; Hansell & Carlson, 1998). According to Hansell & Carlson (1998), DOC_T concentration is about 50 μmol kg^{-1} in freshly formed North Atlantic Deep Water (NADW) east of Greenland. This water is heavily influenced by surface water, which helps explain the elevated DOC_T concentration

relative to other deep water. Hansell & Carlson (1998) found DOC_T in the mid-latitude region of the Atlantic Ocean to be ~43 μmol kg^{-1} and to ~40 μmol kg^{-1} in the Southern Ocean. DOC_T concentration continues to decrease as deep water moves northward through the Pacific Ocean, reaching a minimum concentration of ~34 μmol kg^{-1} off the southern coast of Alaska. This monotonic, decreasing trend in DOC_T indicates that one or more DOC_R degradation processes exists in the deep ocean. Given the slowly evolving nature of the DOC_R pool, illustrated by the low rate of marine DOC_R production (0.043 Pg C yr^{-1}; Hansell, 2013), even a low rate of removal can impact DOC_T dynamics substantially.

Radiocarbon (^{14}C) is produced in the atmosphere, and the relative abundance of ^{14}C in dissolved inorganic carbon (DIC) indicates the ventilation times of water masses in the ocean. Gas exchange between the atmosphere and the surface ocean provides newly produced $^{14}CO_2$ that is quickly converted to $H^{14}CO_3^-$ and $^{14}CO_3^{2-}$ through the carbonate equilibrium reactions. The net atmosphere-to-ocean flux of isotopically young $DI^{14}C$ maintains the most positive (i.e., youngest) $\Delta^{14}C$ values at the ocean surface. It is important to note the testing of atomic weapons throughout the mid 20th century led to an excess of ^{14}C in the atmosphere ("bomb ^{14}C"), which has since penetrated the surface ocean and parts of the deep ocean. This has resulted in anomalously high $\Delta^{14}C$ values, especially in the surface ocean. For example, Broecker & Peng (1982) found $\Delta^{14}C$ in surface DIC to be around +110‰, with the most positive $\Delta^{14}C$ found in the mid-latitudes. After correcting for "bomb ^{14}C", surface DIC $\Delta^{14}C$ dropped to -50‰. Since the conclusion of atomic weapon testing, the abundance of bomb ^{14}C in the atmosphere has steadily declined due to diffusion into the ocean, which is reflected in more recent $\Delta^{14}C$ measurements (+50‰; Druffel et al., 2015; Druffel et al., 2016). Bomb ^{14}C is not incorporated into the model to

be described below. However, bomb ^{14}C has not reached the deep North Pacific (Druffel et al., 2019), which makes it a useful place to compare model output to observation.

Once surface water is advected to the deep ocean (> 1,000 m) and cut off from atmospheric ^{14}C, radioactive decay acts on $DI^{14}C$ along its path through the deep ocean, causing DIC $\Delta^{14}C$ to become more negative (i.e., older). Recent DIC radiocarbon measurements taken in the Atlantic (Druffel et al., 2016), Pacific and Southern Oceans (Druffel et al., 2015) confirm this. DIC $\Delta^{14}C$ of freshly formed North Atlantic Deep Water (NADW) is around +50‰. Traversing the deep ocean pathway, DIC $\Delta^{14}C$ drops to -125‰ in the South Atlantic. In the Southern Ocean, DIC $\Delta^{14}C$ values are around -150‰. The South Pacific Ocean exhibits DIC $\Delta^{14}C$ values around -200‰ and the North Pacific has the most negative DIC $\Delta^{14}C$ values (-250‰) for any marine water mass. Overall, the gradient in DIC from North Atlantic to North Pacific is ~200‰.

The global distribution of $\Delta^{14}C$ in DOC_T generally follows that of DIC because both are transported through the ocean by advection and diffusion. However, DOC_T $\Delta^{14}C$ measurements by Druffel et al. (1992, 2015, 2016) indicate that DOC is older and the gradient between North Atlantic and North Pacific is smaller than for DIC. As with DIC, the youngest DOC_T $\Delta^{14}C$ values are found in the surface ocean, with typical surface DOC_T $\Delta^{14}C$ values across the global ocean near -200‰. $\Delta^{14}C$ values steadily decline with depth until stabilizing around 1,000 m. In the deep ocean, DOC_T $\Delta^{14}C$ becomes increasingly depleted along the deep ocean transit. According to Druffel et al. (2016), NADW has DOC_T $\Delta^{14}C$ values around -400‰ immediately after subduction in the North Atlantic, and -475‰ in the South Atlantic. In the Southern Ocean, Druffel et al. (2015) measured DOC_T $\Delta^{14}C$ values of -500‰, while both the South and North Pacific exhibit DOC_T $\Delta^{14}C$ values around

-525‰. A more recent study by Druffel et al. (2019) shows that DOC_T $\Delta^{14}C$ in the deep North Central Pacific is actually in the range of (-550‰) – (-570‰). Overall, the gradient in DOC from North Atlantic to North Pacific is -150‰, about 50‰ smaller than the gradient for DIC.

The underlying reason for the persistent nature of the DOC_R pool has been a topic of debate for a few decades now. One of the leading explanations is the recalcitrance hypothesis, which posits that a small fraction of DOC_T is resistant to degradation because of the inherent chemistries and molecular structures of its constituents. Calling on the Microbial Carbon Pump (MCP) (Jiao et al., 2010; Jiao et al., 2011), this hypothesis proposes that microbes consume DOC_T and exude structurally and chemically distinct DOC_R. Whereas the Biological Pump mainly concerns new production, the MCP concerns regenerated production, converting low concentrations of reactive DOC to high concentrations of recalcitrant DOC by altering its composition (C:N:P). A critical aspect of the MCP is the Microbial Loop (ML) (Azam et al., 1983), which describes a set of ecological relationships between phytoplankton, bacteria, and flagellates that allow organic and inorganic nutrients to be recycled many times over in the surface ocean. DOC released by phytoplankton is utilized by heterotrophic bacteria, which are subsequently preyed on by flagellates, which are then preyed on by larger predators for a net movement of DOC_T up the trophic pyramid. Predation releases inorganic nutrients back into the water column where they can be fixed by phytoplankton into more organic matter. Therefore, DOC can be processed by the MCP, recycled by the ML, and re-processed by the MCP, leading to the production of increasingly recalcitrant DOC fractions. This constant and efficient reworking of materials results in the production of a fraction of organic carbon, however

small it may be, that is chemically inaccessible to microbes and therefore able to escape the ML. This specific fraction would be exported to the deep ocean as DOC_R.

Additional support for the recalcitrance hypothesis comes from a link between particle size and $\Delta^{14}C$, where the largest organic matter (including both POC and DOC) tends to have the youngest $\Delta^{14}C$ ages (Amon & Benner, 1996; Walker et al., 2016a,b). This size-age link supports the idea that organic matter is broken down over time from POC to successively smaller DOC, as heterotrophic bacteria consume and break down sinking POC. It has also been shown that the C:N:P ratio of DOC_R (3,511:202:1) is much higher than the C:N:P for DOC_L (199:20:1) or POC (106:16:1) (Jiao et al., 2010). The large deviation of DOC_R stoichiometry from that of more fresh organic matter indicates preferential remineralization of nutrients N and P over C through repeated consumption. The C:N:P stoichiometry of DOC_R thus may indicate the chemical compositions which are less energetically favorable (i.e., refractory) to microbes.

The dilution hypothesis, another explanation for the persistence of DOC_R, argues that DOC_T is inherently labile but so chemically and structurally diverse that the concentration of a specific DOC_T structure is too low for any microbe to effectively utilize it (Arrieta et al., 2015). The enormous diversity of DOC_T is indicated by the fact that while less than 10% of the DOC pool has been analytically characterized, thousands of molecules have already been identified based on mass spectrometer analysis (Hertkorn et al., 2006). This means that the concentration of individual types of DOC_T molecules will be on the order of picomoles kg^{-1}. Lechtenfeld et al. (2015) showed that marine microbes produce thousands of structurally unique DOC compounds after being fed only simple organic molecules, which provides a mechanism for the incredible diversity. Furthermore, Arrieta

et al. (2015) showed that deep ocean microbial communities, which did not grow under *in situ* conditions, grew measurably when deep water was concentrated. These results suggest that perhaps no matter what the molecular structure, if the concentration of a specific DOC_T molecule is high enough, it will be metabolized by microbes. Despite the recent effort to reconcile the recalcitrance and dilution hypotheses (Jiao et al., 2018), it remains to be seen whether or to what degree they complement each other in explaining the persistent nature of DOC_R.

Photodegradation in the surface ocean is widely considered to play a critical role in removal of marine DOC_R (Benner & Biddanda, 1998; Mopper et al., 1991; Stubbins et al., 2012). The importance of photodegradation is indicated by the significant compositional differences between surface and deep DOM. Surface ocean DOM is enriched in lower molecular weight compounds with relatively lower amounts of C and H compared to deep ocean DOM. In addition, deep ocean DOM is characterized by high levels of Polycyclic Aromatics (PCA's) and aromatic compounds in general, which are highly photodegradable (Stubbins et al., 2012; Stubbins & Dittmar, 2015). Conversely, surface ocean DOM is enriched with unsaturated aliphatic compounds, which have been shown to be photoproduced compounds. These compositional differences lead to the conclusion that upon upwelling and exposure to irradiation, DOC_R from depth is transformed either to DIC or more labile organic forms (DOC_{SL} and DOC_L) (Medeiros et al., 2015). An abiotic photodegradation pathway would remineralize DOC_R directly to DIC in the form of CO and CO_2. In a second photodegradation pathway, DOC_R is transformed into DOC_{SL} and DOC_L, which are then metabolized to DIC by heterotrophic microbes. The combined magnitude of the two photodegradation pathways is estimated to be at least equivalent to

the annual global input of riverine DOC_T (0.21 Pg C yr^{-1}; Dai et al., 2012) (Miller et al., 2002; Wang et al., 2004).

Measurements of DOC_T concentration and $\Delta^{14}C$ at depth suggest that some DOC_R must also be degraded in the deep ocean. Hydrothermal systems have been shown to alter the major and minor components of seawater (Mottl & Holland, 1978; Seyfried & Mottl, 1982; Seyfried, 1987), which has made them a primary focus for deep ocean DOC_T degradation (Lang et al, 2006; McCarthy et al, 2011; Hawkes et al, 2015; Druffel & Griffin, 2015). Broadly speaking, there are three different types of hydrothermal systems and their net effect on DOC_T varies (Lang et al, 2006). High-temperature vents (black smokers) are considered to be sinks for DOC_R, removing an estimated 0.7-1.4x10^{10} g DOC_R yr^{-1} from the deep ocean through thermal ablation. Diffuse vents are thought to be sources of DOC_T to the deep ocean, perhaps through biological production and desorption from subsurface sediments, providing an estimated 3-28x10^{10} g DOC_R yr^{-1}. However, the estimated DOC_R fluxes for high-temperature and diffuse vents pale in comparison to that of off-axis vents (2.3x10^{12} g DOC_R yr^{-1}) due to greater seawater flux. Off-axis vents process ~1,000 times more seawater (4.8x10^{16} kg_{sw} yr^{-1}; Johnson & Pruis, 2003) than high-temperature vents (3.0-5.9x10^{13} kg_{sw} yr^{-1}; Mottl, 2003). Since off-axis vents typically exist many kilometers away from the ridge axis, seawater circulating in these vents must travel along an extended subsurface pathway compared to high-temperature and diffuse vents. The resulting elongated vent residence time (~10^3 years; Walter et al, 2018), combined with cooler fluid temperatures, makes sorption to minerals and heterotrophic consumption likely processes for DOC_T removal.

While our understanding of ocean DOC_T has advanced significantly in recent years, DOC_T remains difficult to characterize analytically because of its diverse chemistry and structure. Furthermore, incubation experiments require months to years to reveal information about the reactivity of DOC's various fractions. In this study, we took a modeling approach to complement observational studies. Our goal is to gain a global perspective on the important sources and sinks of DOC_R that can help explain large scale observations of DOC_T concentrations and $\Delta^{14}C$, and we build on previous model studies that have represented or examined DOC in more limited ways. For example, Yamanaka and Tajika (1997) employed a global ocean model with two DOC pools with spatially uniform degradation timescales to examine photodegradation as a potentially important DOC degradation mechanism. Murnane et al. (1999) included a semi-labile DOC fraction in a global model meant to examine the significance of the biological pump in air-sea CO_2 fluxes. Bendtsen et al. (2002) also focused on photodegradation using a global model implemented with a mechanistic microbial loop to explain the elevated DOC concentration in the North Atlantic. Using a box model, Hansell et al. (2012) modeled three DOC fractions (semi-labile, semi-refractory, and refractory) with the goal of estimating DOC removal rates that are consistent with DOC distributions. More recently, Letscher et al. (2015) applied variable stoichiometry to a DOM pool within a global ocean model to examine the impact of variable stoichiometry on export production. Wilson and Arndt (2017) used a one-box model of the deep ocean box to test the validity of the dilution hypothesis of DOC_R and found the hypothesis capable of explaining the observed $\Delta^{14}C$ values of DOC with judicious choice of the dilution threshold estimate (the DOC concentration below which microbial consumption does not occur).

This study employs a 3D earth system model with well-calibrated deep ocean ventilation and explicitly represents DOC_{SL} and DOC_R fractions. We represent DOC production occurring in the surface ocean and at depth from the degradation of sinking POC. DOC removal varies spatially, with photodegradation at the surface, hydrothermal degradation around vents, and general background degradation everywhere else in the ocean. We focus on the dynamics of the DOC_T pool over tens of thousands of years, with an emphasis on the relative contributions of suspected removal processes.

2. Methods

2.1. MESMO 2

The model used in this study is the second version of Minnesota Earth System Model for Ocean biogeochemistry (MESMO 2), an intermediate complexity earth system model (EMIC) (Matsumoto et al., 2008; 2013). MESMO 2 has a 3D dynamical ocean, energy-moisture balance atmosphere, dynamic and thermo-dynamic sea ice, and marine biogeochemistry. The ocean component of the model is a 36x36 equal area grid with 10° increments in longitude, and latitude increments ranging from ~3° at the equator to ~20° at the poles. There are 16 depth levels in MESMO 2 that increase in layer thickness with depth. There are two layers in the top 100 m where biological production takes place. MESMO 2 is well calibrated with respect to deep ocean ventilation in terms of $\Delta^{14}C$ values of DIC and the uptake of transient tracers like CFCs and anthropogenic carbon.

As an EMIC, MESMO 2 occupies a modeling niche that allows it to provide ocean dynamics and spatial resolution that box models cannot, without requiring the significant computational resources of high-resolution comprehensive coupled models. This is a

critical advantage for studying DOC_T in a 3D model. For example, a 6,010 year spin up run performed with NCAR's Community Earth System Model with a 3º grid resolution took 7 months of constant running on a supercomputer and global DOC_T $\Delta^{14}C$ values had yet to satisfy the criterion for steady state of <0.001% drift in $\Delta^{14}C$ (Jahn et al., 2015). In comparison, the same simulation in MESMO 2 would take ~7 hours of wall time (~70 minutes per 1,000 years). With MESMO 2 we are thus able to reach steady state, which is necessary to properly study DOC_T $\Delta^{14}C$ (Jahn et al. 2015) and conduct multiple sensitivity experiments. For this study, MESMO 2 runs were performed between 20,000 and 50,000 years until the slowly evolving DOC_R reservoir reached steady state.

In the biological formulation of MESMO 2 (Matsumoto et al., 2013), two size classes of phytoplankton carry out primary production in the top two layers. Production is limited by the nutrient in the shortest supply among phosphate, nitrate, iron, as well as silicic acid for the large phytoplankton class. Production further depends on ice cover, light availability, mixed layer depth, and temperature. Prior to the model modifications described in subsequent paragraphs, organic carbon consisted of POC and a short-lived DOC (effectively DOC_{SL}). Organic carbon production was divided between POC and DOC according to a prescribed split (F_{DOC}) of 1:2 (Yamanaka & Tajika, 1997). POC was directly remineralized to DIC as it sank through the water column. DOC was prescribed a timescale of decay on the order of a few months, allowing it to accumulate only in the upper ~500 m.

2.2. New DOC Modeling Features

New features were added to MESMO 2 in this study to introduce DOC_R and represent a more complete ocean DOC_T cycle (Fig. 1). The salient features of the DOC_T-enabled model are summarized in Table 1 and described below. Table 1 also lists the observational constraints on key model parameters as "Literature Values" and calibrated parameter values as "Tuned Values."

2.2.1. Temperature and Primary Production dependent F_{DOC}

Instead of having a global prescribed value for F_{DOC}, the DOC versus POC split of primary production is now formulated as a function of primary production and temperature according to Dunne et al. (2005). According to the new F_{DOC} formulation, local F_{DOC} ranges from 0.28-0.72%, where low primary production and high ocean temperature favor of DOC. Without the new formulation, surface DOC_T concentrations essentially mimic the Primary Production signal, with excessively high concentrations at the equator and subpolar waters and low concentrations at the mid-latitudes. The new formulation effectively smooths out the DOC_T distribution in the surface ocean, which better matches observed spatial patterns (Hansell, 2013).

2.2.2. Addition of the DOC_R Pool

We now have two fractions of DOC: DOC_R and DOC_{SL}, and consequently a new parameter (F_{DOCr}) was created to determine the split between DOC_{SL} and DOC_R production (Fig. 1). The magnitude of F_{DOCr} is poorly constrained by direct observation due to the difficultly in measuring the concentrations of distinct DOC fractions *in situ*, but previous modeling efforts have found that a split of roughly 99:1 between DOC_{SL}:DOC_R reproduces

the observed DOC distribution reasonably well (Yamanaka & Tajika, 1997; Hansell, 2013). Similarly, an incubation experiment with artificial seawater inoculated with a marine microbial assemblage showed a split of 99.4:0.6 (Osterholz et al., 2015). Our choice of F_{DOCr} (Table 1) is guided by these studies.

Here, DOC_R has a general background decay timescale on the order of 10^4 years to represent slow removal in the interior ocean, as well as two more specific decay timescales representing photodegradation and hydrothermal vent degradation.

2.2.3. Conversion of POC to DOC_T at depth

In previous versions of MESMO, sinking POC was remineralized directly to DIC. Here, sinking POC is converted to DOC_{SL} and DOC_R according to F_{DOCr}. This was done in an effort to more accurately represent the current understanding that POC is broken down into DOC.

2.2.4. Photodegradation of DOC_R

Photodegradation of DOC_R is represented in the model by τ_{photo}, a degradation timescale on the order of a few hundred years for DOC_R in the top layer of the ocean model where light intensity is greatest. The basic method for calculating the approximate timescale for photodegradation (to be more carefully tuned later) was derived following Yamanaka & Tajika (1997), who calculated the residence time of DOC_R in the surface ocean by assuming all DOC_R removal occurs in the surface ocean via photodegradation. In this case, the residence time must be much shorter than the global DOC_R turnover time to reflect the significantly smaller size of the surface ocean relative to the total ocean.

Yamanaka & Tajika accounted for this by combining the global marine DOC_R turnover time with the ratio of average surface depth to average ocean depth to estimate a degradation timescale of ~70 years in the surface ocean (Eq. 1).

$$\tau_{DOC_R,surface} = 5000\ yrs\ \times \frac{50\ m}{3700\ m} \approx 70\ yrs \quad (1)$$

Here we tailored Eq. 1 for MESMO 2 (Eq. 2). Instead of assuming the global ocean to be 1D (Eq. 1), we take a 3D approach by finding the ratio of surface depth (45 m) to total depth ($depth_{ij}$) at each grid point. Also, an average residence time of 5,600 years (Druffel et al., 1992) was used instead of 5,000 years. These adjustments result in a τ_{photo} of 120 years. As with the calculation by Yamanaka & Tajika (1997), this result assumes that DOC_R is degraded exclusively via photodegradation so a τ_{photo} <120 years would not make physical sense.

$$\tau_{photo} = 5600yrs \times \frac{1}{N} \int_{i=1}^{36} \int_{j=1}^{36} \frac{45m}{depth_{ij}} \approx 120\ yrs \quad (2)$$

The daily average light threshold, above which photodegradation occurs in MESMO, is set to 5 Wm^{-2}. The low threshold essentially allows photodegradation to occur ubiquitously in the surface ocean and accounts for the fact that MESMO is driven by daily average insolation. In our formulation DOC_R is directly converted to DIC instead of DOC_{SL}, because $\tau_{sl} << \tau_{bg}$ and any DOC_{SL} created during this process would be rapidly converted to DIC.

2.2.5. Hydrothermal vent degradation of DOC_R

As described above, hydrothermal vents were implemented as a DOC_R degradation process. In our model, this degradation occurs in grid locations that correspond to known ridges [Beaulieu et al., 2015]. The annual global seawater flux through vents (H_{flux}) of $4.8x10^{16}$ kg_{sw} yr^{-1} (Table 1) is divided equally amongst all prescribed ridge locations. We assume seawater that goes through the vents will lose all DOC_R. The vent grid cells have a total seawater mass which is much greater than the prescribed seawater mass that fluxes through vents in those cells in one model timestep (~10^{21} kg vs. ~10^{13} kg). Therefore, the seawater mass in the vent grid cells that does not flux through the vents is subjected to background degradation with τ_{bg}.

2.3. Observational Targets

To assess how well these literature values can explain observations of DOC_T and to further develop a well-calibrated model of DOC_T, we compare our model results to four key observational targets (Table 2): (1) surface DOC concentration; (2) deep ocean DOC concentration, (3) the gradient in DOC concentration along the deep ocean pathway, and (4) deep Pacific $\Delta^{14}C$ values. Here, the deep ocean pathway is defined as beginning with deep water formation in the North Atlantic and ending in the North Pacific. The deep gradient is calculated as the percent difference in DOC concentration between the North Atlantic and North Pacific at 3,000 m, which assumes that any change in deep ocean DOC concentration is a result of the background decay (τ_{bg}) and hydrothermal vent degradation (τ_{vent}).

3. Model Results

3.1. Literature Value Run (LVR)

LVR (experiment 811012c) was simulated with MESMO with key DOC model parameters set to the literature values (Table 1). Since there is little in the literature to constrain τ_{vent}, the parameter was set to 0.05 years, which is short enough to completely remove DOC_T in seawater passing through vents in a single timestep (MESMO time step is 0.05 years). The aim of LVR was to evaluate how well the model simulates the four observational targets with the currently available knowledge. The LVR model output (Figure 2) exhibits large deviations from observation for all key targets selected for this study except $\Delta^{14}C$ of DOC_T. Most notably, Figure 2a shows that DOC_T concentrations are an order of magnitude higher than observation in both the surface (~300 μM vs. 60-80 μM) and deep ocean (~160 μM vs. 35-40 μM) reported by Hansell (2013). In addition, the LVR deep ocean gradient in DOC_T is only 14%, less than half the observed 29% (Hansell & Carlson, 1998), which indicates sluggish DOC_T removal in the modeled deep ocean. Relative to DOC_T concentration, LVR model output for $\Delta^{14}C$ values (Fig. 2b) compares more favorably to observations made by Druffel et al. (1992), showing approximately -230‰ (observations=-190‰,) in the surface ocean and -520‰ (-550‰ to -570‰) in the deep ocean. An important note on radiocarbon in the model is that DIC is less depleted along the deep ocean pathway in MESMO 2 (-120‰) than is observed (-200‰). To account for this, all reported DOC $\Delta^{14}C$ values have had an additional 80‰ subtracted so that comparison to observation is valid.

As previously stated, our simulations do not account for bomb $\Delta^{14}C$, which is present in modern observations. Bomb $\Delta^{14}C$ drives $\Delta^{14}C$ (especially in the surface ocean) to more positive values, which explains why surface DOC $\Delta^{14}C$ in the model is depleted relative to observations. Bomb $\Delta^{14}C$ has not reached the deep Pacific though (Druffel et al., 2019), so the model-observation mismatch in deep Pacific $\Delta^{14}C$ listed above is significant and represents a shortcoming in the model configuration.

The inability of the model to reproduce the large-scale distributions in DOC_T concentration and $\Delta^{14}C$ indicates that the key model parameters obtained from the literature are either not applicable to the global ocean or as of yet unidentified DOC_T sink or source terms are missing from the model. Assuming the former for now, we seek a set of model parameters that would yield more reasonable DOC_T concentrations and ages. Tuning was guided by the analysis of LVR and systematically sweeping the parameter space with ensemble model runs, with the goals of understanding the sensitivity of our model results to our choice of DOC model parameters and creating an optimum overall match between observations and model output with respect to the four targets (Table 2).

3.2. Tuned Run (TR): The tuned model

The DOC model parameters were tuned with the goal of bringing model output closer to observations (Table 1), resulting in TR (experiment 901012c) The most pronounced parameter changes are a six-fold reduction of F_{DOCr} and a four-fold increase in H_{flux}. Smaller changes include a 50% increase in τ_{bg} and a 50% increase in τ_{photo}. The results of TR are in better agreement with observations than LVR for all key targets except $\Delta^{14}C$. Surface and deep DOC concentrations (Fig. 3a) are consistent with observed

concentrations of approximately 70 and 35 μmol kg^{-1}. The deep ocean DOC_T gradient shows a 25% reduction in DOC_T concentration from the deep North Atlantic to the deep Pacific (Fig. 3a), which compares favorably to the observed 29%. TR $\Delta^{14}C$ of DOC_T (Fig. 3b) are slightly depleted relative to observations in the surface ocean (-230‰ vs. -190‰), but this can be largely attributed to the absence of the bomb component. However, deep Pacific $\Delta^{14}C$ values have deviated further from observations (-470‰ vs. -550‰~-570‰) than in LVR (-520‰ vs. -550‰ to -570‰), which cannot be explained by the bomb component.

3.3. Sensitivity Tests

Sensitivity tests were performed to examine the sensitivity of every target to changes in F_{DOCr}, τ_{bg}, τ_{photo}, and H_{flux}. τ_{DOCsl} was not included because it is relatively inconsequential for DOC_T cycling. Also, τ_{vent} was not included because it is treated as a constant due to lack of literature constraint. In Figures 5-8, the parameter space around the TR parameter values was explored by varying each parameter from 1-200% of their TR value. The entire parameter space is shown in these figures so the behavior of the model can be better understood, but analysis is guided using literature values as lower limits for τ_{bg} (16,000 yrs) and τ_{photo} (120 yrs). These lower limits were implemented on the basis that values lower than these would result in an even greater deviation from observed $\Delta^{14}C$. Furthermore, a τ_{photo} of 120 represents complete DOC removal via photodegradation in the surface ocean, so values below this threshold would not make physical sense. The upper limits for τ_{bg} and τ_{photo} are assumed to be the end of the parameter space (48,000 years and 360 years), three times the literature values.

The effects of parameter variation on surface DOC_T concentration show that TR surface DOC_T concentration (~64 μmol kg^{-1}) falls on the lower edge of the acceptable region (60-80 μmol kg^{-1}) (Figure 4). Surface DOC_T concentration is at its lowest (<20 μmol kg^{-1}) when F_{DOCr} is small (Fig. 4a,b), and at its highest (~130 μmol kg^{-1}) when F_{DOCr} is large (enhanced DOC_R production, Fig. 4a,b). Large τ_{bg} (Fig. 4a) and τ_{photo} (Fig. 4b) also result in elevated surface DOC_T concentration, but to a lesser extent than F_{DOCr}. For example, doubling F_{DOCr} results in a 75% increase in surface DOC_T concentration while doubling τ_{photo} (τ_{bg}) only results in a 14% (5%) increase. Conversely, doubling H_{flux} results in an 18% decrease in surface DOC_T concentration (Fig 4c). These results demonstrate that surface DOC_T concentration is primarily controlled by DOC_R production (i.e., F_{DOCr}) and secondarily by vent degradation.

The results of the sensitivity tests for deep DOC_T concentration show that it has similar controls as surface DOC_T concentration (Fig. 5). TR deep DOC_T concentration (~40 μmol kg^{-1}) lies on the upper end of the acceptable region in all subplots. As with the surface, deep DOC_T concentration is most dependent on F_{DOCr} (doubling results in 98% increase in deep DOC_T concentration, Fig. 5a), followed by H_{flux} (32% decrease with doubling, Fig. 5c), τ_{photo} (19% increase with doubling, Fig. 5b), and τ_{bg} (10% increase with doubling, Fig. 5a).

As for the deep DOC_T gradient, H_{flux} is clearly the most influential parameter in the model (Figure 6). TR deep gradient (~24%) lies below the observed value (29%). The deep gradient is highest when H_{flux} is large and τ_{bg} is small. Doubling H_{flux} results in a 54% increase in the deep DOC_T gradient, while doubling τ_{bg} only causes a 7% decrease (Fig. 6c). The deep gradient is entirely insensitive to changes in F_{DOCr} (Fig. 6a,b), while τ_{photo}

minimally affects it (doubling results in 1% increase, Fig. 6b). So, while surface and deep DOC_T concentration are dependent on all four selected parameters, the deep DOC_T gradient is predominately influenced by H_{flux}, with a minor contribution from τ_{bg}.

The sensitivity of deep Pacific DOC_T $\Delta^{14}C$ to the selected parameters is shown in Figure 7. TR $\Delta^{14}C$ (~-470‰) is quite distant from the literature value (-550‰ to -570‰). $\Delta^{14}C$ is at its lowest when the sinks for DOC_R are small (small H_{flux}, Fig. 7c; large τ_{bg} and τ_{photo}, Fig. 7d). Like the deep DOC_T gradient, deep Pacific DOC_T $\Delta^{14}C$ is independent from F_{DOCr} (Fig 7a,b) and H_{flux} is the most influential parameter for deep Pacific DOC_T $\Delta^{14}C$, with smaller contributions from τ_{photo} and τ_{bg}. Doubling H_{flux} causes $\Delta^{14}C$ to become younger by 19%. In the model, τ_{photo} and τ_{bg} are less important in controlling the deep Pacific DOC_T $\Delta^{14}C$; doubling them causes $\Delta^{14}C$ to become older by only 7% and 4%, respectively (Fig. 7d).

Figures 4-7 can be used to further constrain model parameter values obtained from the literature (Table 1). For surface DOC_T concentration, the acceptable range corresponds to an F_{DOCr} range of 0.15-0.25% (Fig. 4a) and 0.14-0.29% (Fig. 4b), and an H_{flux} range of 1.0-3.0x10^{17} $kg_{sw}yr^{-1}$ (Fig. 4c). For τ_{photo}, only a lower bound of 125 years can be determined because the acceptable range is not completely captured in the parameter space (Fig. 4d). From the sensitivity plots for deep DOC_T concentration, an acceptable F_{DOCr} range of 0.14-0.19% (Fig. 6a) and 0.13-0.21% (Fig. 5b) are deduced. The acceptable range for H_{flux} is 1.3-2.4x10^{17} $kg_{sw}yr^{-1}$ (Fig. 5c) and that for τ_{photo} is 125-275 years (Fig. 5d). The deep DOC_T gradient indicates that the acceptable H_{flux} range is 2.5-3.0x10^{17} $kg_{sw}yr^{-1}$ (Fig. 6c). The acceptable region in Fig. 6b is completely outside of the parameter space, which means $\tau_{photo} > 360$ years. From the deep Pacific DOC_T $\Delta^{14}C$ sensitivity plots, we find the

acceptable H_{flux} range to be 0-0.6x10^{17} $kg_{sw}yr^{-1}$ (Fig. 8c), $\tau_{photo} > 360$ (Fig. 7d), and $\tau_{bg} > 48{,}000$ (Fig. 7a). Such large values for τ_{photo} and τ_{bg} are beyond the upper bounds defined above and seem highly unrealistic. The TR value for deep Pacific $\Delta^{14}C$ deviates significantly from observation while TR values for the other key targets are in general agreement with observation, which strongly suggests that the greatest deficiency of the model is related to processes that control $\Delta^{14}C$, and it is likely that a key process is missing.

4. Discussion

LVR output exhibits large mismatches from observations, especially DOC_T concentrations and deep DOC_T $\Delta^{14}C$ gradient. Modeled DOC_T concentrations in the surface and deep ocean are an order of magnitude too high, and the deep DOC_T gradient is half the observed value. Tuning resolved deviations in concentration but was unable to do the same for radiocarbon age. The discussion is subdivided to address the implications of those results. Parts I and II discuss suggested changes to literature values for H_{flux} and F_{DOCr}, respectively, based on successful tuning of parameter values. Part III discusses processes missing from MESMO that could contribute to satisfying the radiocarbon age constraint. Part IV introduces potential directions for future work.

4.1. Deep DOC gradient & H_{flux}

The logical place to begin parameter tuning was to focus on the deep DOC_T gradient because it depends on the least number of parameters (largely dependent on H_{flux} with a minor contribution from τ_{bg}, Fig. 6). Only two possible explanations exist for the insufficient deep DOC_T gradient within the framework of MESMO: a) vent degradation

(H_{flux}) is too low or b) the timescale of background degradation (τ_{bg}) is too high. Figure 6c shows both that H_{flux} is much more significant in establishing the deep gradient than τ_{bg}, and an H_{flux} of ~2.5-3.0x10^{17} $kg_{sw}yr^{-1}$ is required to maintain the observed deep ocean gradient of 29%, independent of any other parameter choice. This H_{flux} is an order of magnitude larger than the maximum literature value (4.8x10^{16} $kg_{sw}yr^{-1}$), even while assuming 100% removal of DOC_R in vents. If modeled DOC_R removal in vents aligned more closely to observation (50%), the required H_{flux} would be even larger.

Literature values for H_{flux} are based on the discrepancy between actual heat flow measurements at the ocean floor and values predicted from thermal models of the cooling lithosphere (Stein & Stein, 1994; Lang et al., 2006), but these estimates have been extrapolated globally from measurements taken from a few locations. Substantial spatial variability in vent types (high-temperature, off-axis, diffuse) and their effect on DOC make it possible that these extrapolations are underestimating the significance of hydrothermal vents in DOC_R removal. For example, if the global heat flow discrepancy is caused by hydrothermal circulation through high temperature vents (350 ºC), Lang et al. (2006) estimates H_{flux} would be 2.9x10^{13} kg_{sw} yr^{-1}. Mottl (2003) estimated a similar value for high temperature vents of 3.0-5.9x10^{13} kg_{sw} yr^{-1}. If, instead, flow through diffuse vents (20 ºC) is assumed, the H_{flux} estimate by Lang et al. (2006) increases by two orders of magnitude to 2.3x10^{15} kg_{sw} yr^{-1}. The largest H_{flux} estimate is for off-axis vents, at 4.8x10^{16} kg_{sw} yr^{-1} (Johnson & Pruis, 2003).

In addition to uncertainties in the magnitude of seawater flux through vents mentioned above, it is unclear what happens to DOC while it passes through vents. Complete ablation at high-temperature vents is perhaps the most intuitive DOC_T

interaction, but sorption to/desorption from sediments and microbial production/consumption are also thought to contribute to varying degrees (Lang et al., 2006) and it is difficult to tease apart these affects. Subsurface DOC interactions are currently poorly understood, but advancements could help clarify the role of hydrothermal vents in DOC_R cycling.

The deep gradient is successfully established in MESMO only with a large H_{flux}, but the required H_{flux} is so large that in TR hydrothermal vent degradation accounts for ~50% of the total DOC_R removal (with 30% coming from photodegradation and 20% from background decay). This goes against the current understanding that photodegradation, not hydrothermal vents, are the most significant sink for DOC. Furthermore, Hansell et al. (2013) argue that hydrothermal vents only account for 4% of the global removal of exported DOC_R. However, many of the ocean's hydrothermal vent fields have yet to be discovered and examined, and with this progress will come more certainty and perhaps a new way of thinking about their significance in DOC_T cycling.

The modeling work presented here suggests that hydrothermal vents are not only helpful, but necessary in maintaining the deep ocean DOC gradient, but if the key to the deep ocean DOC_T gradient lies elsewhere, then perhaps DOC_T adsorption to sinking particles or the formation of organic gels from DOC_T (Verdugo & Santchi, 2010) may provide a solution.

4.2. DOC concentration & F_{DOCr}

We suggest two possible explanations for the oversized DOC_T pool in LVR: a) degradation of DOC_R is too slow, b) production of DOC_R is too high, or some combination

of both. In the case where slow degradation is the issue, decreasing the degradation timescales for τ_{bg} and τ_{photo} would lead to minor increases in concentration, but it would also drive DOC_T $\Delta^{14}C$ to more positive values that are undesirable since LVR already exhibits positive $\Delta^{14}C$ deviations from observation. On the other hand, the sensitivity analyses indicate F_{DOCr} is by far the most influential parameter for DOC_T concentration (surface and deep) and does not affect the deep gradient or deep Pacific $\Delta^{14}C$. These traits make F_{DOCr} an ideal (and necessary) parameter to tune to produce realistic DOC_T concentrations.

Between LVR and TR, F_{DOCr} was reduced by over 5x (Table 1), which resulted in surface and deep DOC_T concentrations consistent with observations (70 and 35 μmol kg^{-1}, respectively; Hansell, 2013). Averaging the F_{DOCr} ranges deduced from Figures 4a,b and 5a,b gives an F_{DOCr} range of 0.14-0.24%. This reduction is 5x less than the 1% used by Hansell (2013) and more than 4-fold smaller than the 0.75% used by Yamanaka & Tajika (1997) These literature values are derived from modeling and are in line with incubation experiments (Brophy et al., 1989; Ogawa et al., 2001). However, there is also evidence to suggest F_{DOCr} should be much smaller than these modeled literature values. A 3-year mesocosm incubation experiment [Osterholz et al., 2015] that analyzed DOC in unprecedented molecular detail found DOC_R production to be between 0.18-0.36% of Net Community Production (NCP), which provides physical context for the current modeling results. Ultimately, the current study suggests that the production of DOC_R is of a much lower magnitude than most literature values. If this is indeed the case, it suggests the capability of the ML to overcome the incredibly small fraction of DOC_T that becomes

DOC_R by continuously recycling DOC_{SL} while producing very small amounts of DOC_R during each iteration of the loop, ultimately resulting in a significant pool of carbon.

4.3. Addressing the $\Delta^{14}C$ mismatch

The deviation between model output and observed values for deep Pacific $\Delta^{14}C$ could not be resolved in the current configuration of MESMO 2 (Fig. 3b & 7) without causing deviations in the other three key targets, so we require a new process. Rather than add a completely new process, we modified the hydrothermal vent sink so it removes $DO^{14}C$ at a higher rate. An acceleration factor (f_{acc}) was added to the natural decay of $DO^{14}C$ in locations where hydrothermal vent degradation occurs so DOC_T passing through vents ages as if it has been entrained in subsurface hydrothermal circulation for an amount of years equal to f_{acc}. This addition was informed by work done by Walter et al. (2018), who measured DOC $\Delta^{14}C$ at two points along a hydrothermal vent system and found the residence time of DOC_T to be ~2,000 years. f_{acc} is limited to radiocarbon, so it does not exert any influence on DOC_T concentration. Vent effluent could also contain radiocarbon-dead DOC_T fixed by subsurface microbes from mantle carbon, which can be represented by an f_{acc} longer than 2,000 years, adding to the aging effect associated with vents.

It is necessary for some DOC_R to survive vent circulation, otherwise all DOC_R would be degraded instead of aged. Therefore, τ_{vent} was increased by a factor of two (τ_{vent} = 0.1 years) so that only half of DOC_R passing through vents is degraded. To isolate the effect of aging, H_{flux} was also increased by a factor of 2 (H_{flux} = 3.84×10^{17} kg_{sw} yr^{-1}. In other words, slower degradation in vents is counteracted by a larger seawater flux, resulting in a net neutral effect on modeled DOC_T concentration. The overall trend in the results

(Fig. 8) is that a larger f_{acc} results in older deep Pacific $\Delta^{14}C$ values and if τ_{vent} were increased further so that more DOC_T survived hydrothermal vent circulation, the aging effect would be magnified. The key to the aging effect, though, is the contribution of radiocarbon-dead carbon DOC_T in the vent effluent. Even a small contribution has the potential to drive $\Delta^{14}C$ to much more negative values.

4.4. Future directions

The design of this study assumes that DOC_T remineralization follows the Recalcitrance Hypothesis, where DOC_R escapes rapid metabolism due to its inherent structure and chemistry causing it to become inaccessible to microbes. Within this framework, DOC_T spends the bulk of its lifetime being remineralized very slowly in the deep ocean (background degradation), with periods of accelerated remineralization related to exposure to capable degradation processes (photodegradation, vent alteration, ideally suited microbial metabolism, etc.). Shen and Benner (2018) propose that if DOC_T cycling operates with this spatial dependence, then the magnitude of the DOC_T pool should scale with the Meridional Overturning Circulation (MOC). This was not addressed in the current study, but the current configuration of MESMO could be used to examine this hypothesis by varying only the strength of the MOC and analyzing the response of the DOC_T pool.

Another future topic could be modeling DOC_T following the Dilution Hypothesis, where DOC_T cycling is driven by its own concentration. Rather than having process-dependent remineralization timescales, DOC_T remineralization would have one remineralization timescale that scales with its local concentration. Lower DOC_T concentrations would result in lower DOC_T remineralization rates, and a threshold

concentration would define the concentration beneath which remineralization does not occur. A potential future study could evaluate the viability of the Recalcitrance and Dilution Hypotheses by running MESMO under each scenario and comparing how well their results explain key observational targets, as well as how sensitive those results are to changes in model parameters.

5. Conclusions

Our modeling results suggest that marine DOC_T concentration is controlled by initial DOC_T production in the surface ocean and the magnitude of this production is overestimated in the literature by 4-5 times. Additionally, the modeled deep ocean DOC_T gradient cannot be maintained without an H_{flux} that is about an order of magnitude larger than the highest literature estimate. Finally, a combination of radiocarbon-dead DOC_T and DOC_T aged along the vent circulation pathway may help resolve the question of how DOC_T has an old apparent radiocarbon age. Ideally, these model-based suggestions will motivate the collection of more DOC observations, especially those related to hydrothermal vents, that will provide some clarity on these still open-ended questions.

6. Figure Descriptions

Figure 1: Schematic diagram of model additions

Illustration of MESMO model development with regards to DOC. In previous versions (left panel), Organic Carbon was formed based on primary production and a prescribed split sent ~1/3 to POC and ~2/3 DOC_{SL}. POC sank through the water column and was ultimately remineralized to DIC, while DOC_{SL} was quickly remineralized to DIC in the surface ocean. In the new version of MESMO (MESMO2; right panel), a new, longer-lived DOC fraction is added (DOC_R). Organic Carbon formation still depends on primary production, but the POC/DOC split is no longer prescribed and instead depends on temperature and primary production. The split between DOC_{SL} and DOC_R is prescribed. Sinking POC is now converted to DOC and subsequently split between DOC_{SL} and DOC_R, rather than being remineralized directly to DIC. Three sinks were implemented, photodegradation in the surface ocean, degradation associated with hydrothermal vents, and a generic background degradation everywhere else.

Figure 2: LVR output

3a) DOC_T concentration ($\mu mol\ kg^{-1}$)

Longitudinally averaged DOC_T concentration in both the surface and deep ocean for the Atlantic, Southern, and Pacific Ocean basins. DOC_T is an order of magnitude higher than observation. DOC_T concentration decreases from the North Atlantic to the North Pacific at about half the observed rate. Black regions indicate the ocean floor.

3b) $DOC_T\ \Delta^{14}C$ (‰)

Longitudinally averaged DOC_T $\Delta^{14}C$ in both the surface and deep ocean for the Atlantic, Southern, and Pacific Ocean basins. DOC_T radiocarbon values generally agree with observation, with slightly positive (negative) deviation in the surface (deep).

Figure 3: TR output

4a) DOC Concentration ($\mu mol\ kg^{-1}$)

Longitudinally averaged DOC_T concentration in both the surface and deep ocean for the Atlantic, Southern, and Pacific Ocean basins. DOC_T concentration in both the surface and deep ocean is consistent with observation. In addition, the DOC_T gradient from the North Atlantic to the North Pacific agrees with observation.

4b) DOC $\Delta^{14}C$ (‰)

Longitudinally averaged DOC_T $\Delta^{14}C$ in both the surface and deep ocean for the Atlantic, Southern, and Pacific Ocean basins. DOC_T radiocarbon values in the surface ocean generally agree with observation, but deep ocean values are ~150‰ younger than observation have deviated further from observation relative to LVR results.

Figures 4-7: Sensitivity Tests

Model sensitivity tests showing which combinations of key parameter values result in model output that is reasonably close to observational constraints. The axes are the four most significant parameters for DOC_T cycling (F_{DOCr}, H_{flux}, τ_{photo}, and τ_{bg}), and the contour lines represent the model output for the four target observations (Surface [DOC_T], Deep

[DOC_T], Deep Δ[DOC_T], and Deep Pacific $\Delta^{14}C$. The gray shading indicates where model output agrees with observation. The "x" in the center of each plot indicate the TR.

Figure 8: Potential Resolution to $\Delta^{14}C$ Conundrum

Deep Pacific $\Delta^{14}C$ values become older with accelerated DOC_R ageing in vents. An f_{acc} of 2,000 years means that the radioactive decay of $DO^{14}C_R$ circulating through vents is accelerated so that DOC_R exiting hydrothermal vents is 2,000 years older in $\Delta^{14}C$ age than DOC_R entering vents. The range of f_{acc} explored here is much greater than the observed vent circulation time (2,000 years) to account for the contribution of radiocarbon-dead DOC_T fixed from mantle carbon.

7. Figures

Table 1: Key model parameters *Note: $DOC = DOC_{SL} + DOC_R$

Parameter	Tuned Value	Literature Value	Primary Reference
F_{DOC}	N/A	$0.28 < F_{DOC} < 0.72$)	Dunne et al., 2005
F_{DOCr}	0.175%	1%	Hansell, 2013
τ_{DOCsl}	0.0833 yrs (1 mo)	1.5 yrs	Hansell, 2013
τ_{bg}	24000 yrs	16000 yrs	Hansell, 2013
τ_{photo}	180 yrs	70 yrs	Yamanaka & Tajika, 1997
τ_{vent}	0.05 yrs	N/A	N/A
H_{flux}	1.92×10^{17} kg_{sw} yr^{-1}	4.8×10^{16} kg_{sw} yr^{-1}	Lang et al., 2006

Table 2: Key Observational Targets *Note: $DOC = DOC_{SL} + DOC_R$

Target	Literature Value	Primary Reference
Surface [DOC_T] (0-200 m)	60-80 μmol kg^{-1}	Hansell, 2013
Deep [DOC_T] (1000-6000 m)	35-40 μmol kg^{-1}	Hansell, 2013
Deep Δ[DOC_T]	29% reduction	Hansell & Carlson, 1998
Deep Pacific $\Delta^{14}C$	-550 to -570‰	Druffel et al., 2019

Figure 1: Schematic Diagram of Model Additions

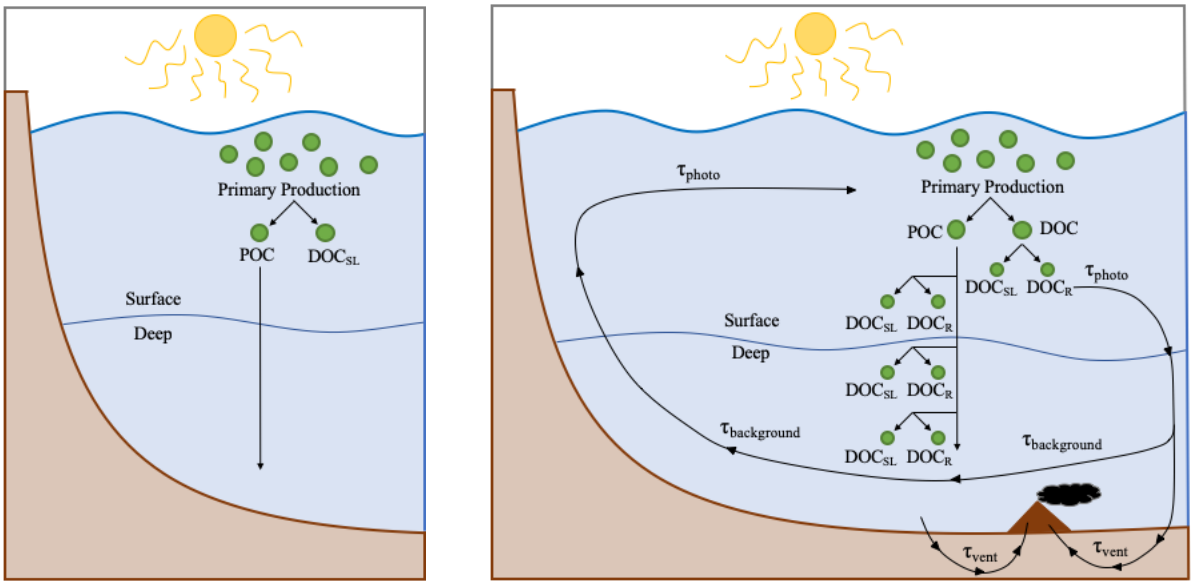

Figure 2: Literature Value Run

(a) DOC_T concentration

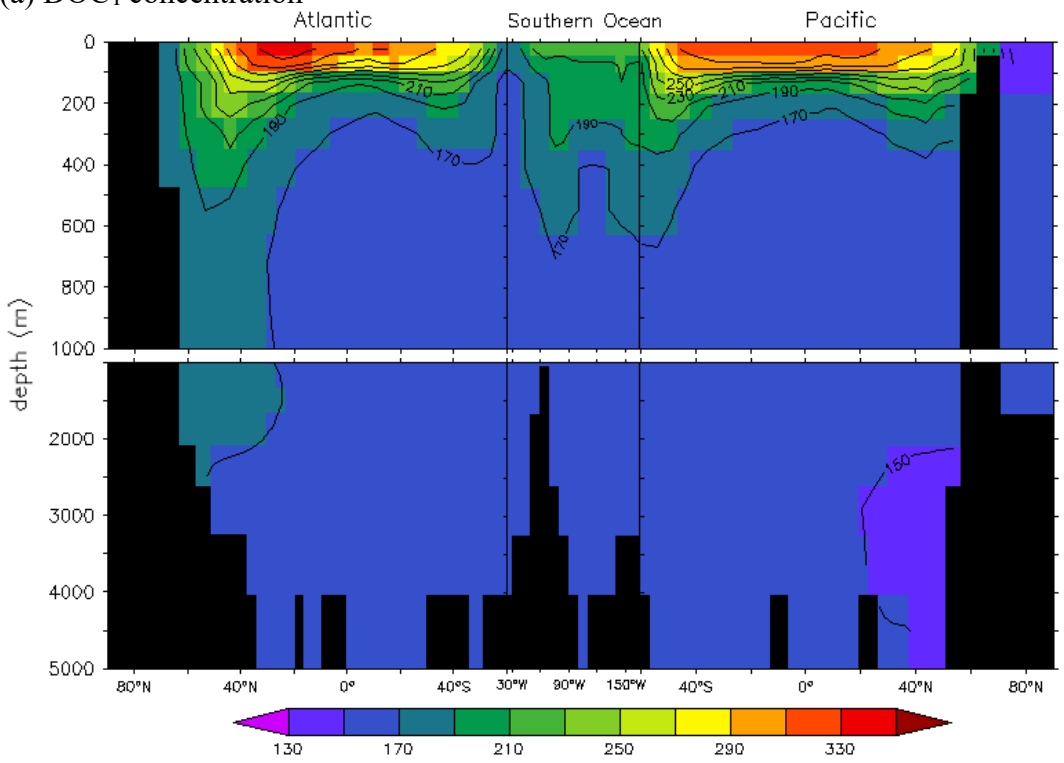

(b) $\Delta^{14}C$ of DOC_T

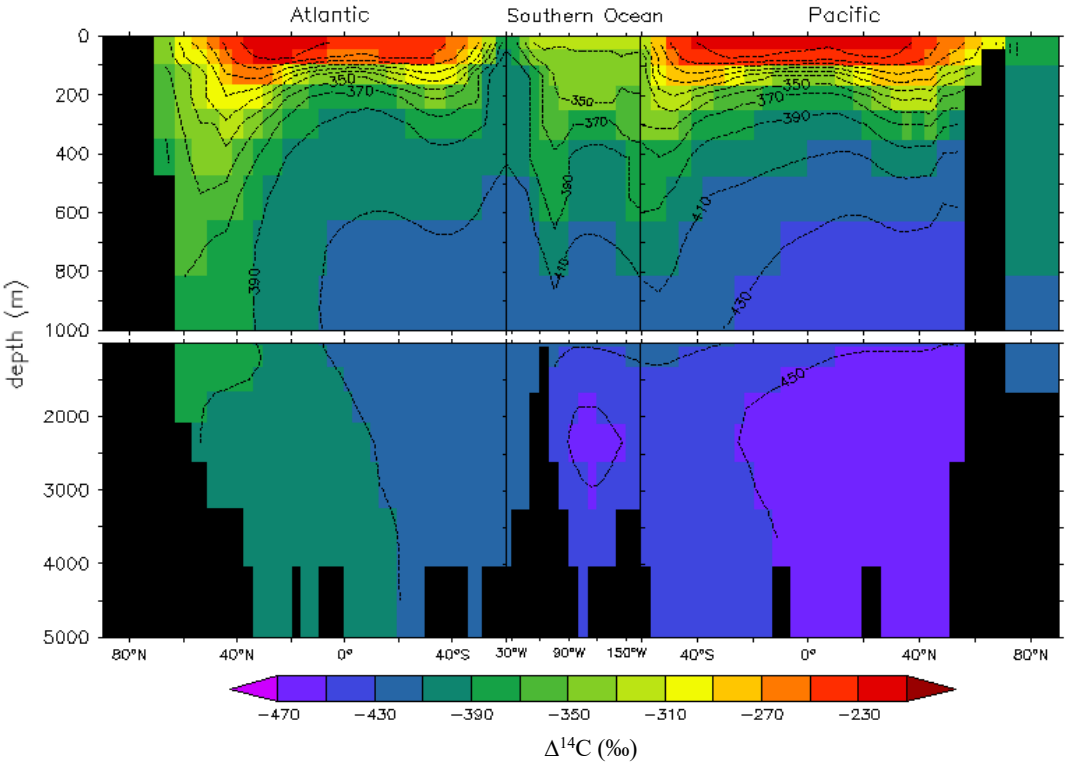

Figure 3: Tuned Run

(a) DOC_T concentration

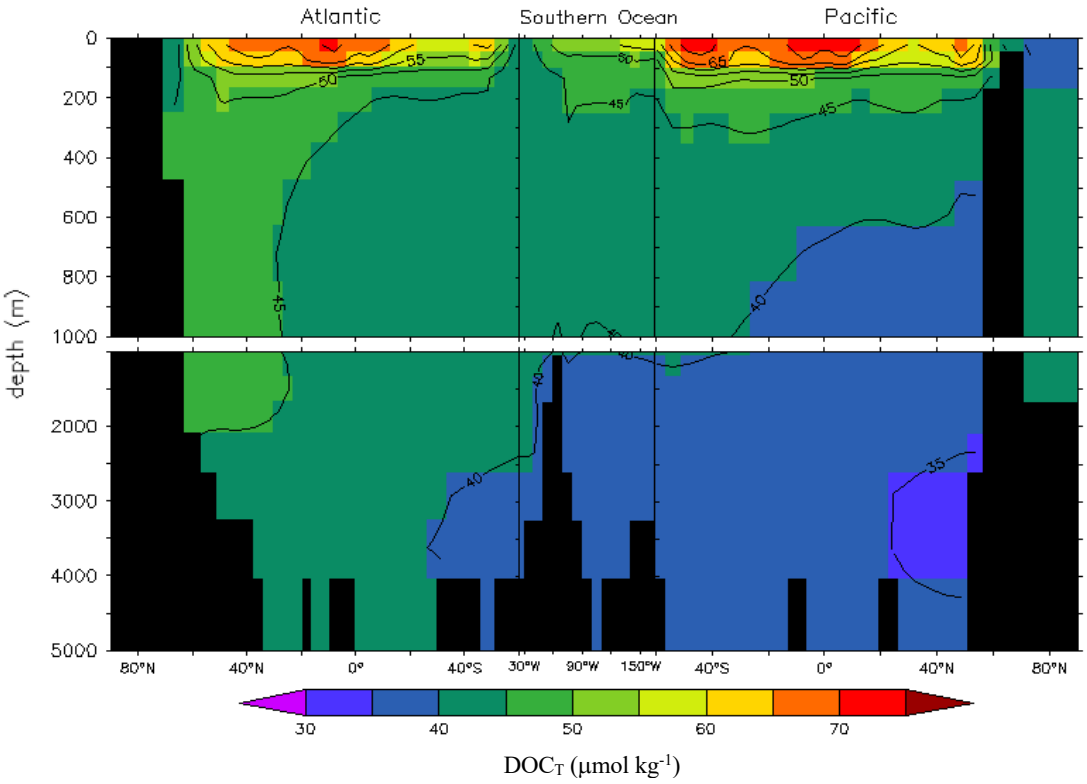

(b) $\Delta^{14}C$ of DOC_T

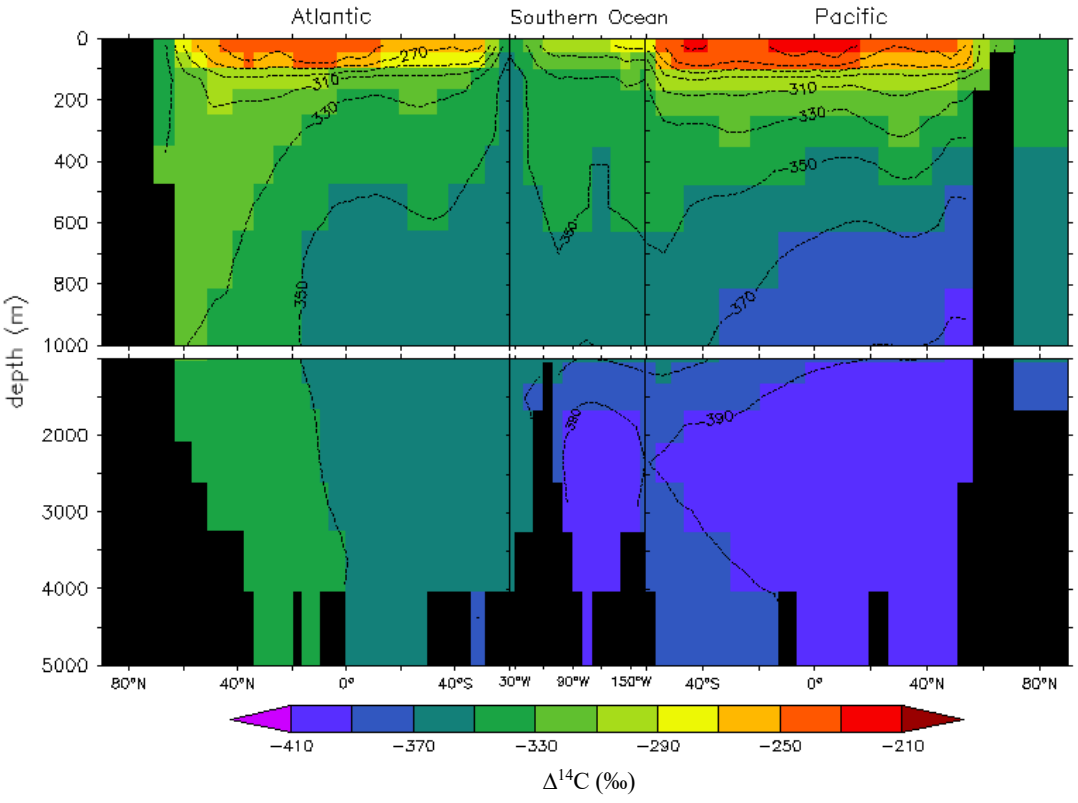

Figure 4: Sensitivity of Surface DOC_T Concentration (μmol kg^{-1})

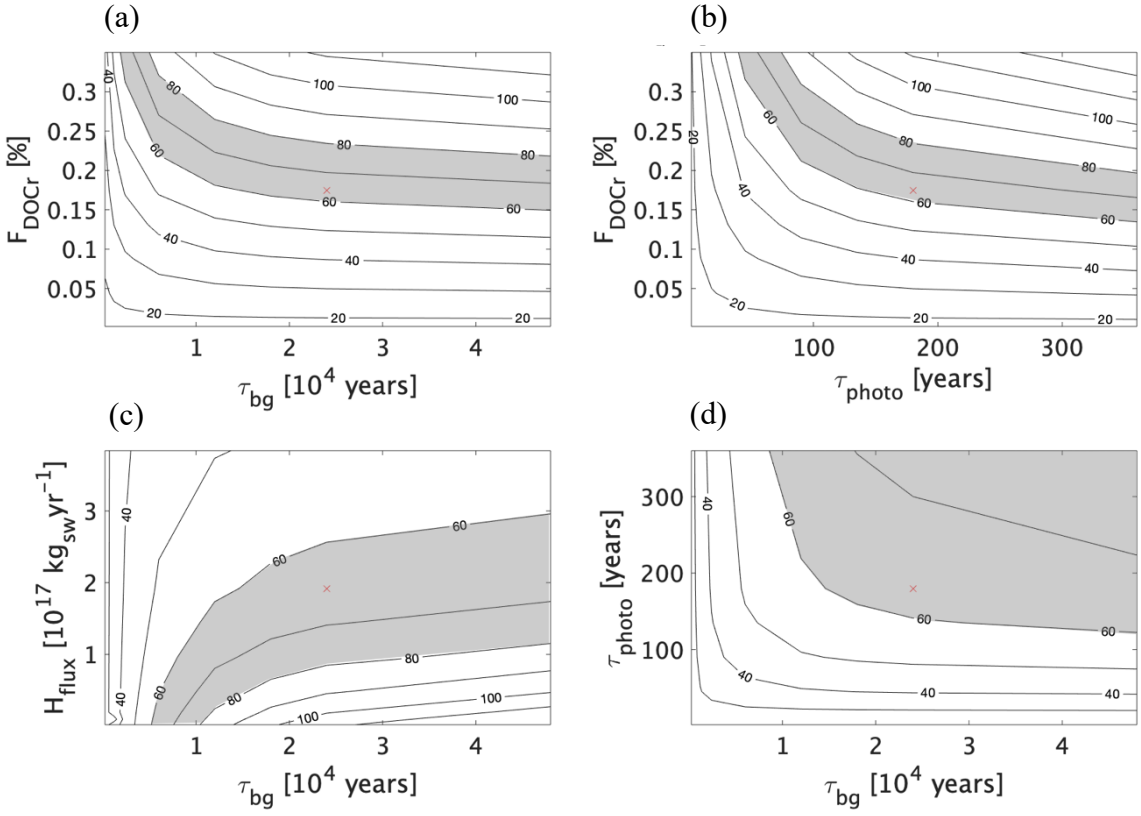

Figure 5: Sensitivity of Deep DOC_T Concentration (μmol kg^{-1})

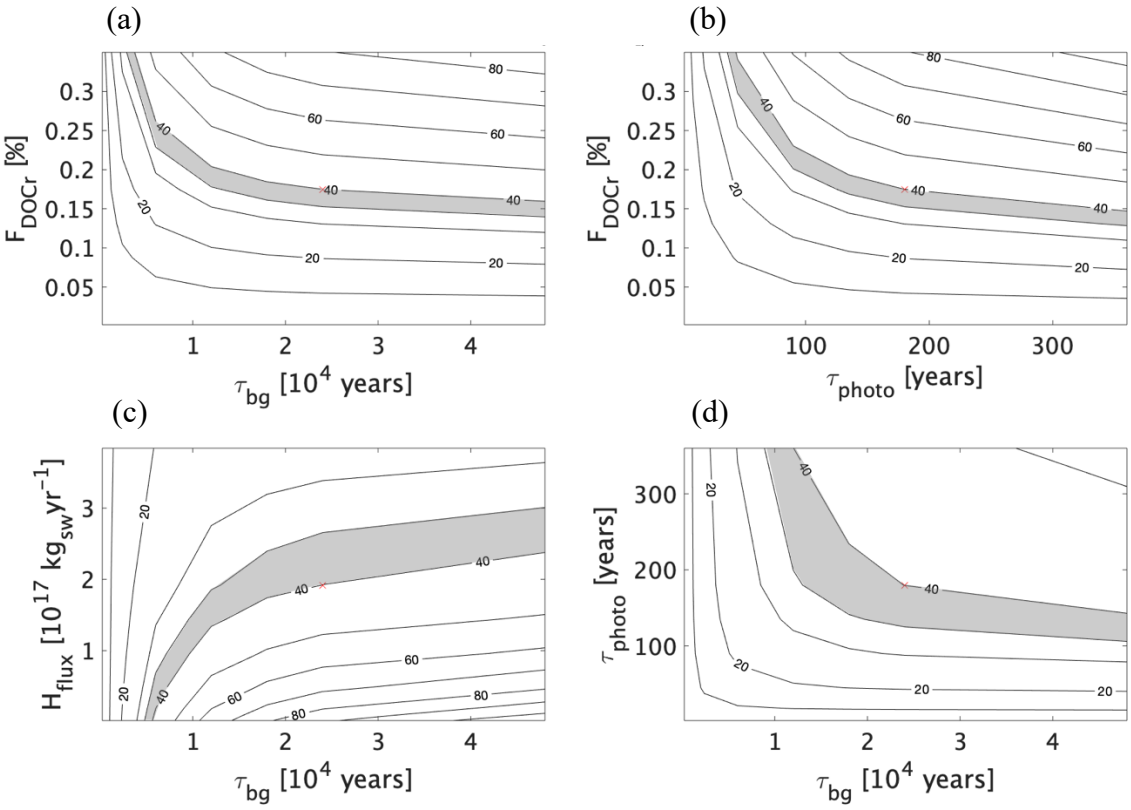

Figure 6: Sensitivity of Deep DOC_T Gradient (%)

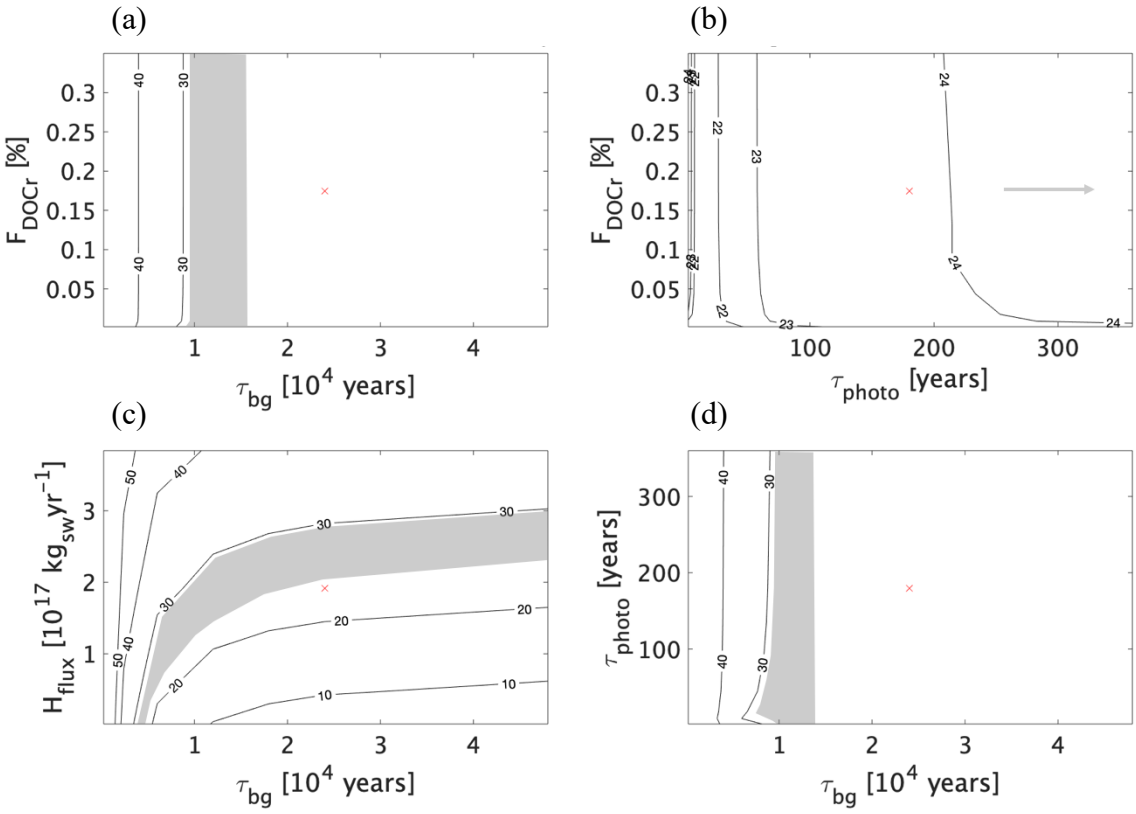

Figure 7: Sensitivity of Deep Pacific DOC_T Δ14C (‰)

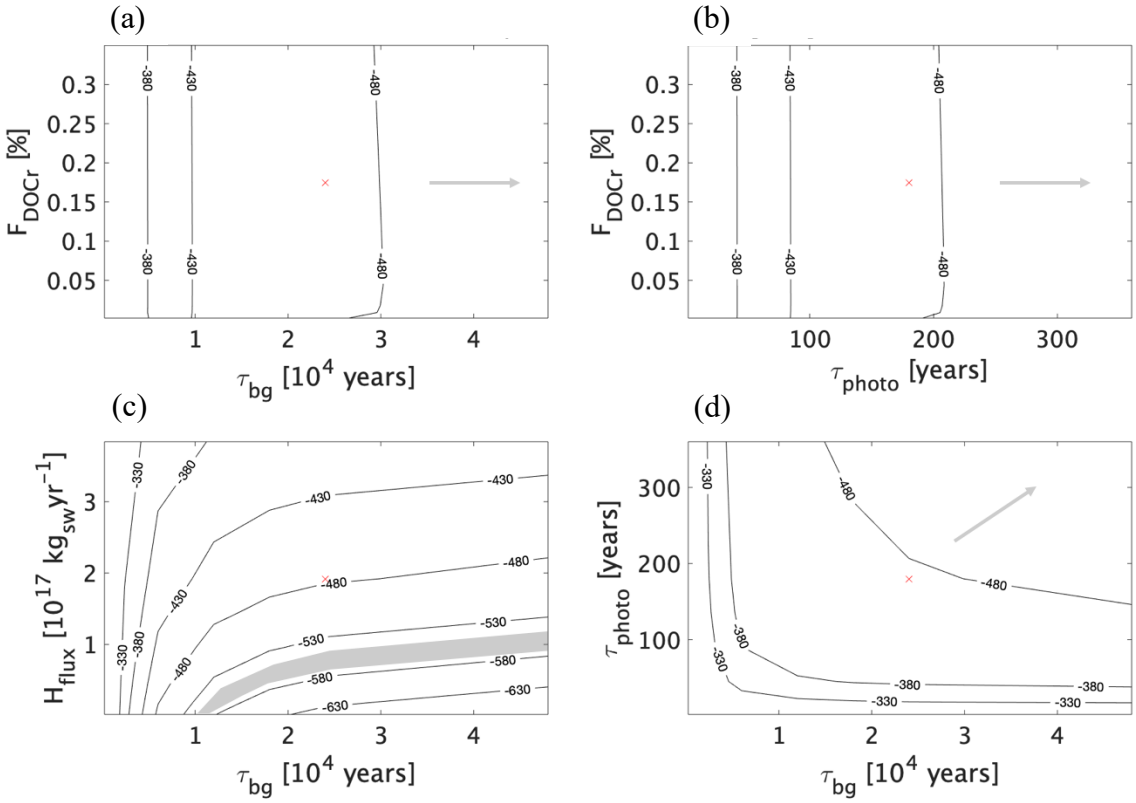

Figure 8: Potential Resolution to $\Delta^{14}C$ Conundrum

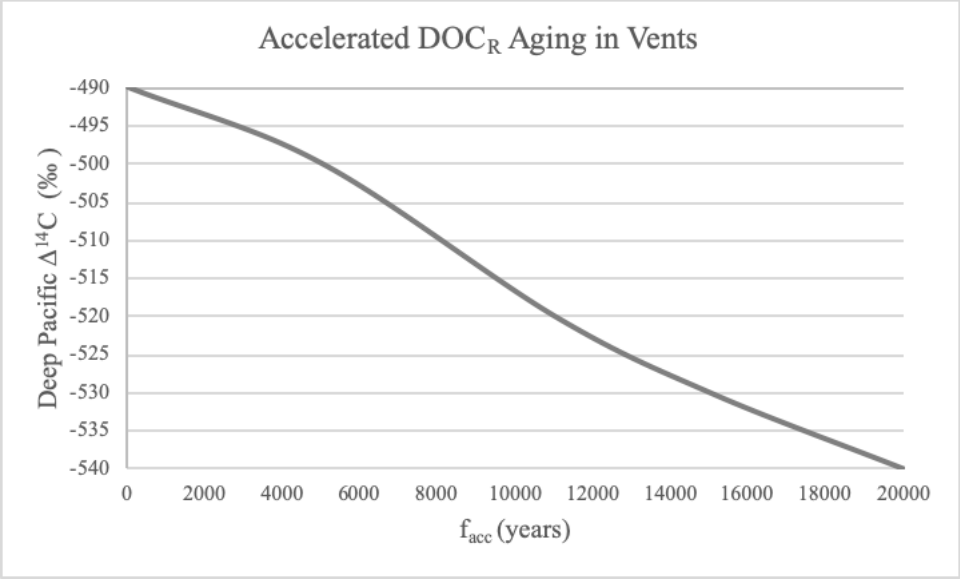

8. Bibliography

Abell J., Emerson S., & Renaud P. (2000). Distributions of TOP, TON and TOC in the North Pacific subtropical gyre: implications for nutrient supply in the surface ocean and remineralization in the upper thermocline. *J. Mar. Res.*, *58*, 203–22

Amon, R.M.W., & Benner, R. (1996). Bacterial utilization of different size classes of dissolved organic matter. *Limnology &* Oceanography, *41*(l), 41–51.

Arrieta, J. M., Mayol, E., Hansman, R. L., Herndl, G. J., Dittmar, T., & Duarte, C. M. (2015). Dilution limits dissolved organic carbon utilization in the deep ocean. *Science*, *350*(6267), 1483b-1484b. https://doi.org/10.1126/science.aac7249

Azam, F., Fenchel, T., Field, J. G., Gray, J. S., Meyer-Reil, L. A., & Thingstad, F. (1983). The Ecological Role of Water-Column Microbes in the Sea. *Marine Ecology Progress Series*, *10*, 257–263. https://doi.org/10.1021/acs.joc.6b00938

Beaulieu, S.E., Baker, E.T., & German, C.R. (2015). Where are the undiscovered hydrothermal vents on oceanic spreading ridges? *Deep-Sea Research Part II: Topical Studies in Oceanography*, *121*, 202–212. doi: 10.1016/j.dsr2.2015.05.001

Bendtsen, J., Lundsgaard, C., Middelboe, M., & Archer, D. (2002). Influence of bacterial uptake on deep-ocean dissolved organic carbon. *Global Biogeochemical Cycles*, *16*(4), 74-1 - 74-12. doi: 10.1029/2002GB001947

Benner, R., & Biddanda, B. (1998). Photochemical transformations of surface and deep marine dissolved organic matter: Effects on bacterial growth. *Limnology & Oceanography*, *43*(6), 1373–1378. doi: 10.4319/lo.1998.43.6.1373

Breitbart, M., Bonnain, C., Malki, K., & Sawaya, N. A. (2018). Phage puppet masters of the marine microbial realm. *Nature Microbiology*, *3*(7), 754–766. https://doi.org/10.1038/s41564-018-0166-y

Broecker, W. S., & Peng, T.-H. (1982). Tracers In The Sea.

Brophy, J. E., and D. J. Carlson. (1989). Production of biologically refractory dissolved organic carbon by natural seawater microbial populations. *Deep Sea Res. 36*, 497–507.

Dai, M., Yin, Z., Meng, F., Liu, Q., & Cai, W. (2012). Spatial distribution of riverine DOC inputs to the ocean: an updated global synthesis. *Current Opinion in Environmental Sustainability*, *4*(2), 170–178. doi: 10.1016/j.cosust.2012.03.003

Dittmar, T., & Stubbins, A. (2014). Dissolved Organic Matter in Aquatic Systems. In *Treatise on Geochemistry: Second Edition* (Vol. 12, pp. 125–156). doi: 10.1016/B978-0-08-095975-7.01010-X

Druffel, E.R.M., & Griffin, S. (2015). Radiocarbon in dissolved organic carbon of the South Pacific Ocean. *Geophysical Research Letters*, *42*(10), 4096–4101. doi: 10.1002/2015GL063764

Druffel, E.R.M., Griffin, S., Coppola, A.I., and Walker, B.D. (2016), Radiocarbon in dissolved organic carbon of the Atlantic Ocean, *Geophysical Research Letters*, *43*, 5279–5286. doi:10.1002/2016GL068746.

Druffel, E. R. M., Griffin, S., Wang, N., Garcia, N. G., McNichol, A. P., Key, R. M., & Walker, B. D. (2019). Dissolved Organic Radiocarbon in the Central Pacific Ocean. *Geophysical Research Letters*, *46*(10), 5396–5403. https://doi.org/10.1029/2019GL083149

Druffel, E.R.M., Williams, P.M., Bauer, J.E., & Ertel, J.R. (1992). Cycling of Dissolved and Particulate Organic Matter in the Open Ocean. *Journal of Geophysical Research*, *97*(C10), 15,639–15,659. doi: 10.1029/92JC01511

Dunne, J.P., Armstrong, R.A., Gnnadesikan, A., & Sarmiento, J.L. (2005). Empirical and mechanistic models for the particle export ratio. *Global Biogeochemical Cycles*, *19*, GB4026. doi:10.1029/2004GB002390

Dunne, J.P., Sarmiento J.L., & Gnanadesikan A. (2007). A synthesis of global particle export from the surface ocean and cycling through the ocean interior and on the seafloor. *Global Biogeochemical Cycles*, *21*, GB4006. doi:10.1029/2006GB002907

Fasham, M. J. R., Balino, B. M., Bowles, M. C., Anderson, R., Archer, D., Bathmann, U., Boyd, P., Buesseler, K., Burkill, P., Bychkov, A., Carlson, C., Chen, C. T. A., Doney, S., Ducklow, H., Emerson, S., Feely, R., Feldman, G., Garcon, V., Hansell, D., Hanson, R., Harrison, P., Honjo, S., Jeandel, C., Karl, D., Le Borgne, R., Liu, K. K., Lochte, Karin, Louanchi, F., Lowry, R., Michaels, A., Monfray, P., Murray, J., Oschlies, A., Platt, T., Priddle, J., Quinones, R., Ruiz-Pino, D., Saino, T., Sakshaug, E., Shimmield, G., Smith, S., Smith, W., Takahashi, T., Treguer, P., Wallace, Douglas W.R., Wanninkhof, R., Watsen, A., Willebrand, Jürgen and Wong, C. S. (2001) A new vision of ocean biogeochemistry after a decade of the Joint Global Ocean Flux Study (JGOFS). *AMBIO: A Journal of the Human Environment*, 2001 (Sp. No. 10). pp. 4-31.

Fuhrman, J. (1991). Bacterioplankton Roles in Cycling of Organic Matter: The Microbial Food Web. In: Falkowski P.G., Woodhead A.D., Vivirito K. (eds) *Primary Productivity and Biogeochemical Cycles in the Sea. Environmental Science Research*, *43*, Springer, Boston, MA. doi: 10.1007/978-1-4899-0762-2_20

Hansell, D.A. (2013). Recalcitrant Dissolved Organic Carbon Fractions. *Annual Review of Marine Science*, *5*, 421–445. doi: 10.1146/annurev-marine-120710-100757

Hansell, D.A., & Carlson, C.A. (1998). Deep-ocean gradients in the concentration of dissolved organic carbon. *Nature*, *395*, 263–266. doi: 10.1038/26200

Hansell D.A., & Carlson C.A. (2002). *Biogeochemistry of Marine Dissolved Organic Matter*. San Diego: Academic. 774 pp.

Hansell, D., Carlson, C., Repeta, D., & Schlitzer, R. (2009). Dissolved Organic Matter in the Ocean: A Controversy Stimulates New Insights. *Oceanography*, *22*(4), 202–211. doi: 10.5670/oceanog.2009.109

Hansell, D. A., Carlson, C. A., & Schlitzer, R. (2012). Net removal of major marine dissolved organic carbon fractions in the subsurface ocean. *Global Biogeochemical Cycles*, *26*(1). https://doi.org/10.1029/2011GB004069

Hawkes, J.A., Rossel, P.E., Stubbins, A., Butterfield, D., Connelly, D.P., Achterberg, E.P., Koschinsky, A., Chavagnac, V., Hansen, C.T., Bach, W., & Dittmar, T. (2015). Efficient removal of recalcitrant deep-ocean dissolved organic matter during hydrothermal circulation. *Nature Geoscience*, *8*, 856-861. doi: 10.1038/NGEO2543

Hertkorn, N., Benner, R., Frommberger, M., Schmitt-Kopplin, P., Witt, M., Kaiser, K., Kettrup, A., Hedges, J.I. (2006). Characterization of a major refractory component of marine dissolved organic matter. *Geochimica Cosmochimica Acta*, *70*, 2990–3010.

Jahn, A., Lindsay, K., Giraud, X., Gruber, N., Otto-Bliesner, B.L., Liu, Z., & Brady, E.C. (2015). Carbon isotopes in the ocean model of the Community Earth System Model (CESM1). *Geoscientific Model Development*, *8*, 2419–2434. doi: 10.5194/gmd-8-2419-2015

Jiao, N., Herndl, G.J., Hansell, D.A., Benner, R., Kattner, G., Wilhelm, S.W., Kirchman, D., Weinbauer, M.G., Luo, T., Azam, F. (2010). Microbial production of recalcitrant dissolved organic matter: long-term carbon storage in the global ocean. *Nature Reviews Microbiology*, *8*(8), 593–599. https://doi.org/10.1038/nrmicro2386

Jiao, N., & Zheng, Q. (2011). The microbial carbon pump: From genes to ecosystems. *Applied and Environmental Microbiology*, *77*(21). doi: 10.1128/AEM.05640-11

Jiao, N., Cai, R., Zheng, Q., Tang, K., Liu, J., Jiao, F., Wallace, D., Chen, F., Amann, R., Benner, R., Azam, F. (2018). Unveiling the enigma of refractory carbon in the ocean. *National Science Review*, (July). doi: 10.1093/nsr/nwy020

Johnson, H.P., & Pruis, M.J. (2003). Fluxes of fluid and heat from the oceanic crustal reservoir. *Earth and Planetary Science Letters*, *216*, 565–574. doi: 10.1016/S0012-821X(03)00545-4

Lampert, W. (1978). Release of dissolved organic carbon by grazing zooplankton. *Limnology and Oceanography*, *23*(4), 831–834. doi: 10.4319/lo.1978.23.4.0831

Lang, S.Q., Butterfield, D.A., Lilley, M.D., Paul Johnson, H., & Hedges, J.I. (2006). Dissolved organic carbon in ridge-axis and ridge-flank hydrothermal systems. *Geochimica et Cosmochimica Acta*, *70*, 3830–3842. doi: 10.1016/j.gca.2006.04.031

Lancelot, C. (1979). Gross Excretion Rates of Natural Marine Phytoplankton and Heterotrophic Uptake of Excreted Products in the Southern North Sea, as Determined by Short-Term Kinetics. *Marine Ecology Progress Series*, *1*, 179–186. doi: 10.3354/meps001179

Laws E.A., Falkowski P.G., Smith W.O. Jr, Ducklow H., & McCarthy J.J. (2000). Temperature effects on export production in the open ocean. *Global Biogeochemical Cycles*, *14*(4), 1231–1246

Lechtenfeld, O. J., Hertkorn, N., Shen, Y., Witt, M., & Benner, R. (2015). Marine sequestration of carbon in bacterial metabolites. *Nature Communications*, *6*, 6711. https://doi.org/10.1038/ncomms7711

Letscher, R. T., Knapp, A. N., James, A. K., Carlson, C. A., Santoro, A. E., & Hansell, D. A. (2015). Microbial community composition and nitrogen availability influence DOC remineralization in the South Pacific Gyre. *Marine Chemistry*, *177*, 325–334. https://doi.org/10.1016/j.marchem.2015.06.024

Matsumoto, K., Tokos, K.S., Price, A.R., & Cox, S.J. (2008). First description of the Minnesota Earth System Model for Ocean biogeochemistry (MESMO 1.0). *Geoscientific Model Development*, *1*, 1–15. doi: 10.5194/gmd-1-1-2008

Matsumoto, K., Tokos, K., Huston, A., & Joy-Warren, H. (2013). MESMO 2: A mechanistic marine silica cycle and coupling to a simple terrestrial scheme. *Geoscientific Model Development*, *6*, 477-494, doi: 10.5194/gmd-6-477-2013

McCarthy, M.D., Beaupré, S.R., Walker, B.D., Voparil, I., Guilderson, T.P., & Druffel, E.R.M. (2011). Chemosynthetic origin of ^{14}C-depleted dissolved organic matter in a ridge-flank hydrothermal system. *Nature Geoscience*, *4*, 32–36. doi:10.1038/ngeo1015

Medeiros, P., Seidel, M., Powers, L.C., Dittmar, T., Hansell, D.A., & Miller, W.L. (2015). Dissolved organic matter composition and photochemical transformations in

the northern North Pacific Ocean. *Geophysical Research Letters*, *42*, 863–870. doi: 10.1002/2014GL062663.Received

Miller, W.L., Moran, M.A., Sheldon, W.M., Zepp, R.G., & Opsahl, S. (2002). Determination of apparent quantum yield spectra for the formation of biologically labile photoproducts. *Limnology & Oceanography*, *47*(2), 343–352

Mopper, K., Zhou, X., Kieber, R., Kieber, D., Sikorski, R., & Jones, R. (1991). Photochemical degradation of dissolved organic carbon and its impact on the oceanic carbon cycle. *Nature*, *353*, 60-62.

Mottl, M.J. (2003). Partitioning of energy and mass fluxes between mid-ocean ridge axes and flanks at high and low temperature. In: Halbach, P.E., Tunnicliffe, V. Hein, J.R. (Eds.). *Energy and Mass Transfer in Marine Hydrothermal Systems*, pp. 271–286.

Mottl, M. J., & Holland, H.D. (1978). Chemical exchange during hydrothermal alteration of basalt by seawater-I. Experimental results for major and minor components of seawater. *Geochimica et Cosmochimica Acta*, *42*, 1103–1115. doi: 10.1016/0016-7037(78)90107-2

Murnane, R.J., Sarmiento, J.L., & Le Quéré, C. (1999). Spatial distribution of air-sea CO_2 fluxes and the interhemispheric transport of carbon by the oceans. *Global Biogeochemical Cycles*, *13*(2), 287–305. doi: 10.1029/1998GB900009

Ogawa, H., Y. Amagai, I. Koike, K. Kaiser, and R. Benner. 2001. Production of refractory dissolved organic matter by bacteria. *Science, 292*, 917–920.

Osterholz, H., Niggemann, J., Giebel, H.A., Simon, M., & Dittmar, T. (2015). Inefficient microbial production of refractory dissolved organic matter in the ocean. *Nature Communications*, *6*. doi: 10.1038/ncomms8422

Proctor, L.M., & Fuhrman, J.A. (1991). Viral mortality of marine bacteria and cyanobacteria. *Nature*, *343*, 60–62.

Seyfried, W.E. (1987). Experimental and theoretical constraints on hydrothermal alteration processes at mid- ocean ridges. *Annual Review of Earth and Planetary Sciences, 15*, 317–335. doi: 10.1146/annurev.ea.15.050187.001533

Seyfried, W.E., & Mottl, M.J. (1982). Hydrothermal alteration of basalt by seawater under seawater-dominated conditions. *Geochimica et Cosmochimica Acta*, *46*, 985–1002. doi: 10.1016/0016-7037(82)90054-0

Shen, Y., & Benner, R. (2018). Mixing it up in the ocean carbon cycle and the removal of refractory dissolved organic carbon. *Scientific Reports*, *8*(1), 1–9. https://doi.org/10.1038/s41598-018-20857-5

Stein, C. A., & Stein, S. (1994). Constraints on hydrothermal heat flux through the oceanic lithosphere from global heat flow. *Journal of Geophysical Research*, *99*(B2), 3081–3095. https://doi.org/10.1029/93JB02222

Stubbins A., Niggemann J., Dittmar T. (2012). Photo-lability of deep ocean dissolved black carbon. *Biogeosciences*, *9*, 1661–1670. doi:10.5194/bg-9-1661-2012

Stubbins, A., & Dittmar, T. (2015). Illuminating the deep: Molecular signatures of photochemical alteration of dissolved organic matter from North Atlantic Deep Water. *Marine Chemistry*, *177*, 318–324. doi: 10.1016/j.marchem.2015.06.020

Verdugo, P., & Santschi, P. H. (2010). Polymer dynamics of DOC networks and gel formation in seawater. *Deep-Sea Research Part II: Topical Studies in Oceanography*, *57*(16), 1486–1493. https://doi.org/10.1016/j.dsr2.2010.03.002

Walker, B.D., Primeau, F.W., Beaupre, S.R., Guilderson, T.P., Druffel, E.R.M., & McCarthy, M.D. (2016). Linked changes in marine dissolved organic carbon molecular size and radiocarbon age. *Geophysical Research Letters*, *43*, 10,385-10,393. doi: 10.1002/2016GL070359

Walker, B.D., Beaupré, S.R., Guilderson, T.P., McCarthy, M.D., & Druffel, E.R.M. (2016). Pacific carbon cycling constrained by organic matter size, age and composition relationships. *Nature Geoscience*, *9*, 888–891. doi: 10.1038/ngeo2830

Walter, S.R., Jaekel, U., Osterholz, H., Fisher, A.T., Huber, J.A., Pearson, A., Dittmar, T., Girguis, P.R. (2018). Microbial decomposition of marine dissolved organic matter in cool oceanic crust. *Nature Geoscience*, *11*, 334–339. doi: 10.1038/s41561-018-0109-5

Wang, X., Chen, R.F., & Gardner, G.B. (2004). Sources and transport of dissolved and particulate organic carbon in the Mississippi River estuary and adjacent coastal waters of the northern Gulf of Mexico. *Marine Chemistry*, *89*, 241–256. doi: 10.1016/j.marchem.2004.02.014

Wilson, J.D., & Arndt, S. (2017). Modeling radiocarbon constraints on the dilution of dissolved organic carbon in the deep ocean. *Global Biogeochemical Cycles*, *31*(5), 775–786. doi: 10.1002/2016GB005520

Yamanaka, Y., & Tajika, E. (1997). Role of dissolved organic matter in the marine biogeochemical cycle: Studies using an ocean biogeochemical general circulation-model. *Global Biogeochemical Cycles*, *11*(4), 599–612